Nanoscale

Accepted Manuscript

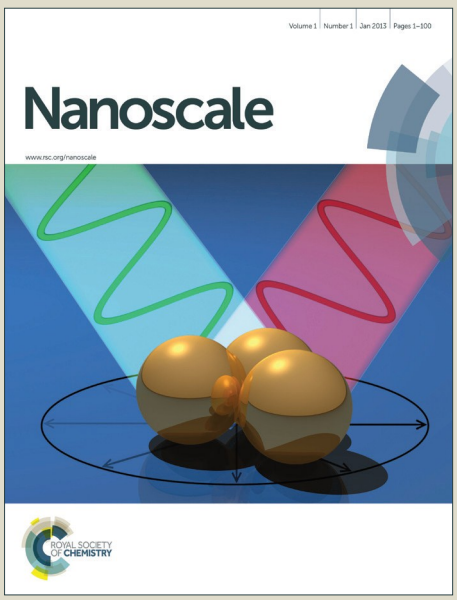

ROYAL SOCIETY OF CHEMISTRY

www.rsc.org/nanoscale

Journal Name

RSCPublishing

ARTICLE

In situ plasmonic Ag nanoparticles anchored TiO_2 nanotube arrays as visible-light-driven photocatalysts for enhanced water splitting

Cite this: DOI: 10.1039/x0xx00000x

Received 00th January 2012,
Accepted 00th January 2012

DOI: 10.1039/x0xx00000x

www.rsc.org/

Ming-Zheng Ge,[a] Chun-Yan Cao,[a] Shu-Hui Li,[a] Yu-Xin Tang,[b] Lu-Ning Wang,[c] Ning Qi,[a] Jian-Ying Huang,*[a] Ke-Qin Zhang,*[a,d] S.S. Al-Deyab[e] and Yue-Kun Lai*[a,d]

An ultrasonication-assisted in situ deposition strategy was applied for the uniform decoration of plasmonic Ag nanoparticles on vertical aligned TiO_2 nanotube arrays (NTAs) to construct Ag@TiO_2 NTAs composite. Ag nanoparticles act as efficient surface plasmon resonance (SPR) photosensitizers for driving photocatalytic water splitting under visible light irradiation. The Ag nanoparticles were uniformly deposited on the surface and inside of the highly oriented TiO_2 nanotubes. The visible-light-driven hydrogen production activities of silver nanoparticles anchored TiO_2 nanotube arrays photocatalysts were evaluated by using methanol as sacrificial reagent in water under a 500 W Xe lamp with a UV light cutoff filter ($\lambda \geq 420$ nm). It was found that the hydrogen production rate of Ag@TiO_2 NTAs prepared by ultrasonication-assisted deposition for 5 min was approximately 15 times higher than that of the pristine TiO_2 NTAs counterpart. The highly efficient photocatalytic hydrogen evolution is attributed to the SPR effect of Ag for enhanced visible light absorption and boosting photogenerated electron-hole separation/transfer. This strategy is promising to design and construct high efficiency TiO_2 based photocatalysts for solar energy conversion.

Faced with the challenge of fossil fuels reduction, human beings have urgently called on the sustainable energy economy. Since hydrogen was envisaged as a clean, renewable and abundant energy source, water splitting for hydrogen production by photocatalysts has become one of the efficient and promising ways to solve the problem of energy shortage in the future.[1,2] Titanium dioxide (TiO_2), since discovered on water photolysis by Fujishima and Honda in 1972,[3] has been paid much attention and widely used in photocatalytic degradation of organic pollutants,[4-7] dye-sensitized solar cells,[8-11] lithium ion batteries [12-15] and hydrogen production by splitting water [16-21] because of its low cost and good mechanical properties. Compared to TiO_2 nanoparticles and nanowires, TiO_2 NTAs vertically oriented on Ti substrate by electrochemical anodization have been paid more attention due to the high specific surface, the oriented charge transfer channel, recyclable and especially rapid electron transfer.[22] However, the wide application of TiO_2 NTAs was limited in some fields suffered from wide band gap (anatase: 3.2 eV, rutile: 3.0 eV) for poor solar light absorption and the fast recombination of photogenerated electron-hole pairs.[23,24]

In recent years, in order to enhance the photoelectric activity of TiO_2 NTAs, many strategies, including doping with other elements such as metal (Au, Fe and Pd),[25-27] nonmetal (N, C and its derivatives),[28-30] semiconductor (CdS, Cu_2O, WO_3 and NiO),[31-33] have been employed to modify TiO_2 NTAs by suppressing the recombination of photogenerated electrons-hole pairs and improving the transport of photocarriers. Especially, noble metal nanoparticles decorated TiO_2 is thought to be one of the most effective strategies to enhance the photoelectric activity due to the SPR effect for optimizing the use of solar energy and improved transfer efficiency of photogenerated carriers.[34-36]

Coupling TiO_2 NTAs with noble metal can form a Schottky barrier, which acts as an electron trapper to prevent electron/hole recombination. Among all noble metals, silver is widely used in photocatalysts because of its much lower cost, non-toxicity and easier get compared with Au, Pd and Pt etc.[37-39] The coupling of TiO_2 NTAs with Ag is a promising strategy for photocatalytic hydrogen production under visible light irradiation because Ag can markedly facilitate the separation of electron and hole at the interface and improve the transfer efficiency of photocarriers. Besides, Ag owns the SPR effect for enhancing visible-light absorption ranging from 400 to 800 nm.[40-42] Recently, there are some reports about Ag@TiO_2 composite nanotube arrays synthesized by photoreduction, electrodeposition and hydrothermal method,[43-46] but exhibit low control over the particle size and dispersion.

Herein, we present an ultrasonication-assisted in situ deposition technique to realize Ag nanoparticles uniformly dispersed on

vertically aligned TiO_2 NATs with a high density. The morphology, structure and photoelectrochemical performance of TiO_2 NTAs with or without Ag nanoparticles loading were systematically investigated and discussed. Compared to pristine TiO_2 NTAs, the Ag@TiO_2 NTAs exhibited higher photocatalytic hydrogen production activity owing to the enhanced visible-light adsorption capacity and higher efficiency of photogenerated charges separation/transfer.

Experimental

Preparation of anodized TiO_2 NTAs: Prior to anodization, titanium foils were ultrasonically cleaned in acetone and ethanol for 20 minutes, respectively. Then cleaned Ti foils (3.0 × 1.5 cm^2) was anodized at room temperature in a conventional two-electrode cell with Pt as counter electrode in ethylene glycol containing 0.5 wt% NH_4F and 2 vol% H_2O. In the first-step anodization, the 50 V potential was applied for 2 h for the growth of nanotubes. The as-anodized Ti foil was then ultrasonically with ethanol to strip the anodized TiO_2 nanotubular layer from the Ti substrate, followed by rinsing with distilled water. Subsequently, the second-step anodization was conducted on the above Ti substrate at 50 V for 5min. Finally, the TiO_2 NTAs was anodized in in ethylene glycol containing 0.5 wt% phosphate acid at 50 V for 5 min in order to enhance the adhesion between the nanotubular layer and substrate. After three-step electrochemical anodization, the samples were rinsed in distilled water and dried in air. The as-prepared amorphous TiO_2 nanotube arrays were annealed in air at 450 ℃ for 2 h with a heating rate and cooling rate of 5 ℃/min to convert to crystalline phases.

Preparation of Ag@TiO_2 NTAs: Ag nanoparticles were loaded onto both the outer and inner walls of TiO_2 nanotubes by the ultrasonication-assisted in situ deposition method. First, 0.1 M ammonia solution was added into 50 ml 10 mM $AgNO_3$ solution. Then, polyvinylpyrrolidone (PVP-K30, 0.4 g) was added to the solution and mixed by an ultrasonic generator (KQ100E, Kunshan Ultrasonic Instrument Co., Ltd) with a frequency of 40 kHz for a few minutes. The resulting solution was heated to 45 ℃ in the water bath. Subsequently, TiO_2 NTAs were immersed into the solution, followed by the addition of 10 ml glucose aqueous solution (0.9 g). After ultrasonication for different time, the samples were rinsed with distilled water to remove NO_3^- ions and glucose. Finally, the samples were dried under vacuum at a temperature of 60 ℃ for 30 min. The corresponding samples were marked as Ag@TiO_2 NTAs-2 to Ag@TiO_2 NTAs-15, respectively. The procedures for the preparation of Ag@TiO_2 NTAs are illustrated in Scheme 1.

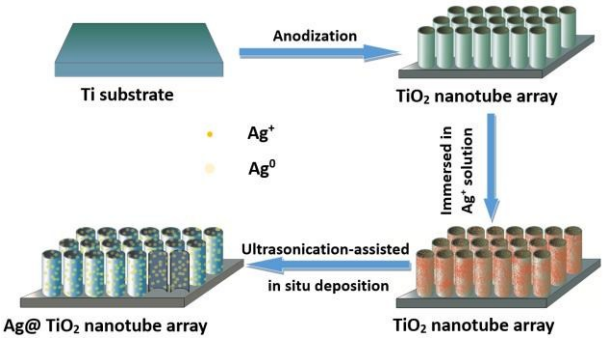

Scheme 1. Schematic diagram of the procedures for preparation of Ag@TiO_2 NTAs.

Characterization of Ag@TiO_2 NTAs: The structure and morphology of Ag@TiO_2 NTAs were characterized by a field emission scanning electron microscope (FESEM, Hitachi-S4800). Energy dispersive X-ray (EDX) spectrometer fitted to the SEM was applied for elemental analysis. The microstructures, compositions and the presence of Ag were further confirmed by using a transmission electronic microscopy (TEM, FEI Tecnai G-20 operated at 200 kV). The crystal phases of the samples were identified by an X-ray diffractometer with Cu-Ka radiation (XRD, Philips, X ́pert-Pro MRD). X-ray photoelectron spectroscopy (XPS, KRATOS, Axis Ultra HAS) was employed to analyze the chemical composition of atoms of Ag@TiO_2 NTAs. The binding energies were normalized to the signal for adventitious C 1s at 284.5 eV. UV-Vis diffuse reflection spectroscopy (UV-DRS) was recorded in range of 200-800 nm at room temperature by using UV-3600 spectrophotometer. Photoluminescence (PL) measurements were carried out at room temperature by using fluorescence spectroscopy (made by HOKIBA JOBIN YVON, FM4P-TCSPC) with a Xenon lamp as excitation source (λ_{ex} = 370 nm). The time-resolved photoluminescence (TRPL) measurements were carried out at room temperature by using fluorescence spectroscopy (made by HOKIBA, FL3-TCSPC) with a Xenon lamp as excitation source (λ_{ex} = 370 nm, 293nm laser).

Photoelectrochemical measurements: The electrochemical impedance spectroscopy (EIS) and photocurrent measurement measures were carried out in a quartz beaker using an electrochemical workstation (PARSTAT 2273) and electrochemical workstation (CHI 660D) in a standard three-electrode configuration with TiO_2 NTAs, Ag@TiO_2 NTAs electrode as the working electrode, respectively. A 0.1 M Na_2SO_4 aqueous solution was used as the electrolyte. The area of working electrodes was 3 cm^2. The working electrode was irradiated with a 150 W xenon lamp with a UV-light cutoff filter ($\lambda \geq 420$ nm) was employed as the visible light source during the measurement. The distance between the window of the flask and light source was 15 cm. The focused incident light intensity on the flask was ca. 60 mW cm^{-2}. The EIS measurements were performed to scrutinize the interfacial properties between the electrode (i.e. TiO_2 NTAs, Ag@TiO_2 NTAs) and the electrolyte over a frequency range from 1 × 10^5 Hz to 0.1 Hz with a low open circuit potential both in the dark and under visible-light illumination.

Photocatalytic hydrogen production measurements: The photocatalytic reactions were carried out in a Pyrex bottom irradiation-type high-throughput photoreactor. The photocatalytic reaction was performed in distilled water containing 20 vol% methanol as the sacrificial agent for the reaction of water splitting producing H_2 only. The active area of the samples was 4.5 cm^2. The reaction solution was initially evacuated to remove air completely and then irradiated from the bottom side by using a 500 W Xenon lamp (Zolix LSP-X500) with a UV light cutoff filter ($\lambda \geq 420$ nm) with the intensity about 80 mW cm^{-2}. A flow of cooling water was used to maintain the reaction mixture at room temperature. The evolved gases were analyzed in a volumetric device with a vacuum line after 4 h illumination.

Results and discussion

Ag incorporated aligned TiO_2 nanotubes was prepared by an ultrasonication-assisted in situ deposition method. Under ultrasonication, the air was expelled from the nanotubes, and Ag^+ ions diffused and penetrated into the nanotubes. After the addition of glucose, Ag^+ ions were in situ reduced to Ag^0 and grew on and inside the TiO_2 nanotubes at the same time. Ag nanoparticles were thus formed as depicted in equation (1).

$$CH_2OH(CHOH)_4CHO+2Ag^+ \xrightarrow{\triangle} CH_2OH(CHOH)_4COONH_4+Ag\downarrow+NH_3+H_2O \quad (1)$$

Figure 1a,b showed the SEM images of pristine TiO_2 NTAs. The TiO_2 NTAs demonstrated a high density, well-ordered, and uniform tubular structure with a length of 2-4 μm and an average pore diameter of 70 nm and a wall thickness of 20 nm. The well aligned highly ordered hexagonal architecture with smooth top surfaces and large porosity is highly favorable for uniform growth of Ag nanoparticles. Figure 1c,d displayed the SEM images of TiO_2 NTAs after in situ growth assisted with optimized ultrasonication deposition time for 5 min. The Ag nanoparticles with an average size of about 8 nm were uniformly deposited on the top of TiO_2 nanotubes and inside the TiO_2 nanotubes. Corresponding EDX analysis and mapping spectra show the as-prepared Ag@TiO_2 NTA sample contains Ti, O and Ag, and the atomic percentage of Ag is 5.24% (Figure S1). Figure 1e displays a representative TEM image of Ag nanoparticles on an individual TiO_2 nanotube, revealing uniform distribution on and inside nanotube with an average size of 8 nm. Figure 1f presents a high magnification TEM image and SEAD spectra of the area marked in Figure 1e. The lattice fringes of 0.351 nm and 0.234 nm corresponded to the reflections from the (101) plane of anatase TiO_2 and (111) plane of Ag, respectively.

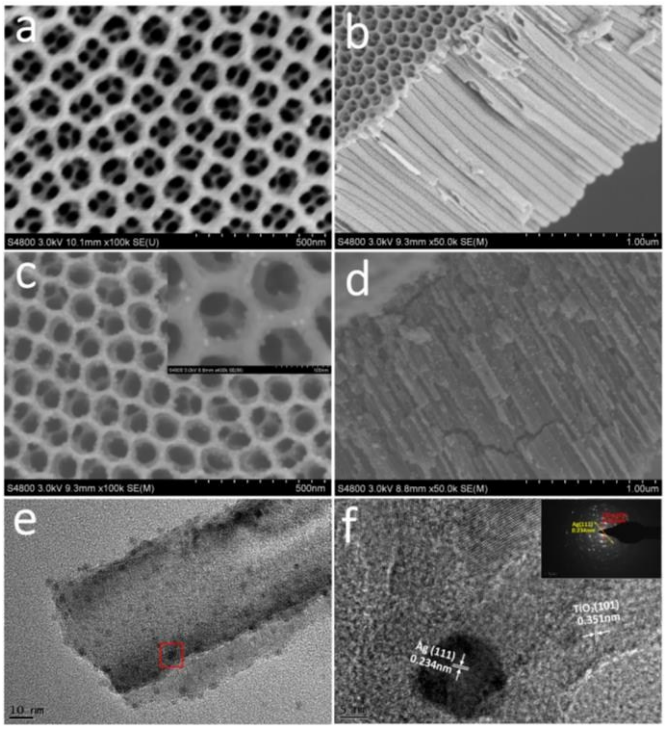

Figure 1. Typical top-view (a) and side-view (b) SEM images of the pristine TiO_2 NTAs. Top-view (c), side-view (d) SEM images, TEM (e), HRTEM images (f) marked in (e) and SAED image (inset f) of Ag@TiO_2 NTAs with optimized ultrasonication-assisted deposition time for 5 min.

Figure 2a-f displayed the top and side view SEM images of Ag@TiO_2 NTAs with ultrasonication-assisted deposition time for 2, 10 and 15 min, respectively. A little amount of Ag nanoparticles was deposited on the surface of TiO_2 NTAs and dispersed mainly around the nanotube entrance with 2 min deposition (Figure 2a). When increasing deposition time, the amount of Ag nanoparticles on nanotube is also markedly increased. The optimized ultrasonication-assisted deposition time is 5 min with a small size of 8 nm. When the deposition time were increased to 10 min, the average size of Ag nanoparticle increased significantly to 28 nm, and some of them even blocked the nanotube entrance (Figure 2c). As time progressed to 15 min (Figure 2e), Ag nanoparticles aggregated to form nanoclusters about 60 nm and most TiO_2 nanotubes were blocked by big nanoclusters. Obviously, in situ growth method assisted with ultrasonication deposition didn't destroy the highly ordered tubular structure of TiO_2 NTAs. Figure S2 shows the size of Ag and mass ratios of Ag, O, and Ti with different ultrasonication-assisted deposition time for 2, 5, 10 and 15 min, respectively. Besides, the concentration of $AgNO_3$ also has much effect on the size of Ag nanoparticles and its hydrogen production activity. A series characterization demonstrated Ag@TiO_2 NTAs with ultrasonication-assisted deposition time for 5 min with 10 mM $AgNO_3$ owns the best photocatalytic hydrogen production activity (Figure S3 to S5).

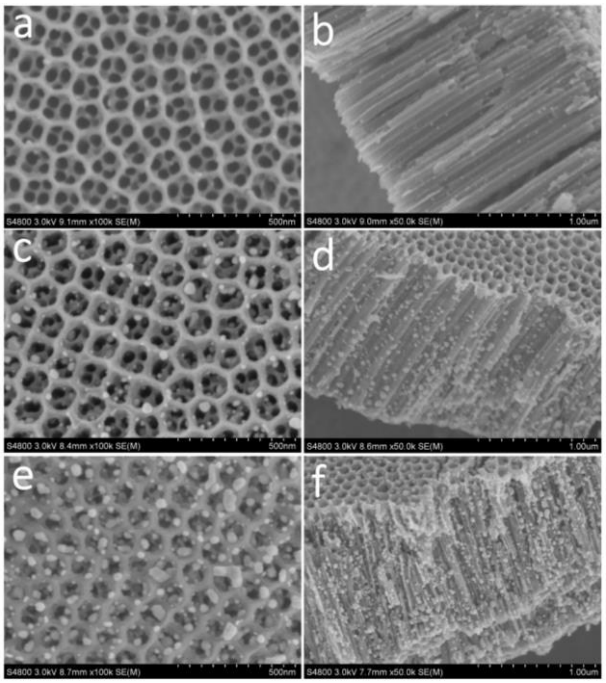

Figure 2. Top-view (a, c, e), side-view (b, d, f) SEM images of Ag@TiO_2 NTAs with ultrasonication-assisted deposition time for 2, 10 and 15 min, respectively.

Figure 3 shows the XRD patterns of the TiO_2 NTAs before and after the deposition of Ag nanoparticles. The diffraction peaks at 25.3 °, 37.9 °, 48.0 ° and 53.9 ° of bare TiO_2 NTAs could be well indexed to the (101), (004), (200) and (105) planes of the TiO_2 anatase phase (JCPDS no. 21-1272). After in situ growth of Ag nanoparticles, there are three peaks at 38.1 °, 44.2 ° and 64.4 ° in accordance with a standard diffraction peaks of Ag (JCPDS no. 04-0783), corresponding to the (111), (200) and (220) plane of Ag, which is consistent with the results of TEM. The strongest peak of Ag (111) is not clear seen as it might be masked by the Ti substrate peak at 38.4 °. And the intensity of the three peaks increased when prolonging deposition time.

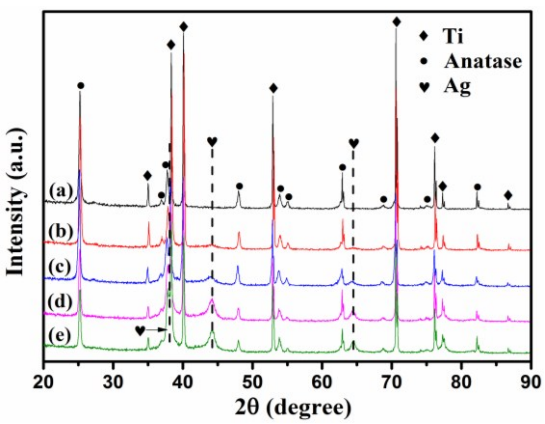

Figure 3. XRD spectra of TiO_2 NTAs at 450 ℃ (a), Ag@TiO_2 NTAs with different deposition time for 2 min (b), 5 min (c), 10 min (d) and 15 min (e).

The chemical composition of Ag@TiO_2 NTAs was analyzed by XPS. Figure 4a,b showed XPS survey spectrum of TiO_2 NTAs and Ag@TiO_2 NTAs. Compared to bare TiO_2 NTAs, it can be seen that except for the O 1s (532.4 eV), Ti 2p (458.9 eV) and C 1s (284.5 eV) peaks, Ag 3d peaks emerged with strong relative intensities, indicating that TiO_2 NTAs were mainly coated with Ag nanoparticles (Figure 4a). The C 1s peak is ascribed to adventitious hydrocarbon from the XPS instrument itself. The higher resolution XPS spectrum of the Ag 3d region is displayed in Figure 4b. The Ag 3d XPS spectra were fitted into two peaks at 368.1 eV (Ag $3d_{5/2}$) and 374.1 eV (Ag $3d_{3/2}$) with the distance approximately 6.0 eV, indicating that Ag mainly exists in the Ag^0 state on the TiO_2 nanotube surface.[47,48]

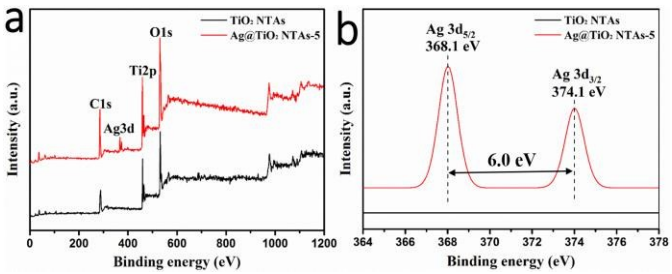

Figure 4. Survey XPS spectrum (a) and high resolution XPS spectra (b) of Ag 3d of pure TiO_2 NTAs and Ag@TiO_2 NTAs with ultrasonication-assisted deposition time for 5 min.

Figure 5a displayed the UV-Vis diffuse reflectance spectra (UV-DRS) of TiO_2 NTAs and Ag@TiO_2 NTAs with different repeated deposition times. The TiO_2 NTAs showed an absorption band lower than 390 nm due to intrinsic band gap absorption of anatase TiO_2.[49-51] Compared to pure TiO_2 NTAs annealed at 450 °C, the TiO_2 NTAs loaded with Ag nanoparticles exhibit a broader absorption in the visible light from 450 nm to 800 nm and the band edges of the samples were approaching the visible-light region owing to the photosensitizing and SPR effect of Ag,[52,53] which means red shift. Usually, the higher absorption toward visible region verified the better photocatalytic activity. Therefore, the Ag@TiO_2 NTAs-5 possessed the strongest absorption among all samples, and thus the highest photocatalytic activity was expected. Figure 5b showed the PL spectra of TiO_2 NTAs and Ag@TiO_2 NTAs with different deposition time. The peaks appeared at about 445 nm, 469 nm, 490 nm and 595 nm, due to the oxygen vacancy of TiO_2 NTAs.[54,55] The lower PL intensity signified that the separation efficiency of photogenerated electron-hole pairs was stronger and the electron was easier to leap the valence band with low energy excitation.[56] Compared with pure TiO_2 NTAs, Ag@TiO_2 NTAs displayed lower PL intensity. The PL intensity decreases in the order of Ag@TiO_2 NTAs-5 < Ag@TiO_2 NTAs-2 < Ag@TiO_2 NTAs-10 < Ag@TiO_2 NTAs-15 < pure TiO_2 NTAs. The increase in the PL signal intensity of the samples obtained with longer deposition time (i.e., Ag@TiO_2 NTAs-15) suggested that the larger Ag nanoclusters might act as the charge recombination center, rather than facilitate electron-hole separation, and partially block the channels of TiO_2 nanotubes. These results indicated that the presence of Ag nanoparticles with optimized size and uniform distribution would suppress the

recombination of electron-hole pairs to endow Ag@TiO_2 NTAs-5 with the best photochemical activity.

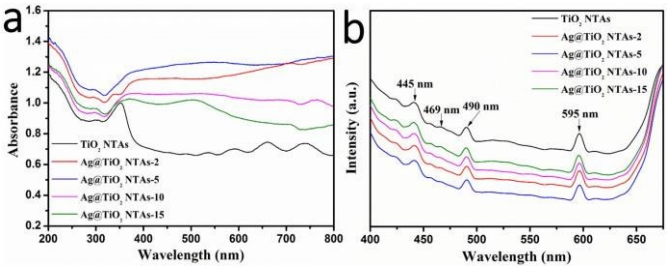

Figure 5. UV-DRS spectra (a) and PL spectra (b) of TiO_2 NTAs and Ag@TiO_2 NTAs with different deposition time for 2, 5, 10 and 15 min.

In order to investigate the charger carrier kinetics and the recombination of electron/holes, time-resolved photoluminescence (TRPL) spectroscopy was performed on TiO_2 NTAs and Ag@TiO_2 NTAs with different deposition time. The time-resolved photoluminescence (TRPL) decay profiles were fitted using the biexponential decay function expressed as follows (Figure 6),[57,58]

$$I(t)=A_1 \exp(-t/\tau_1) + A_2 \exp(-t/\tau_2) \quad (2)$$

The average excited-state lifetime is calculated using the following relationship,[48]

$$\tau_{average}= \sum A_i\tau_i^2 / \sum A_i\tau_i \quad (3)$$

Where A_1 and A_2 are the amplitudes (or weighing factors), and τ_1 and τ_2 are the corresponding lifetimes. As calculated, the average decay lifetime of TiO_2 NTAs and Ag@TiO_2 NTAs with ultrasonication-assisted deposition time for 2, 5, 10 and 15 min are 70.8 ns, 29.8 ns, 28.4 ns 45.8 ns and 68.2 ns, respectively. Compared to the pristine TiO_2 NTAs, Ag@TiO_2 NTAs showed shorter decay lifetime. Longer decay lifetime clearly indicates lower recombination and higer separation efficiency of electron-hole pairs. What's more, lower recombination of electron-hole pairs will lead to weaker photoluminescence and higher photocatalytic activity, which is consistent with the PL spectra.[59] These results reveal that plsamonic Ag nanoparticles can act as electron filters to effectively separate excitons and hinder the charge recombination.

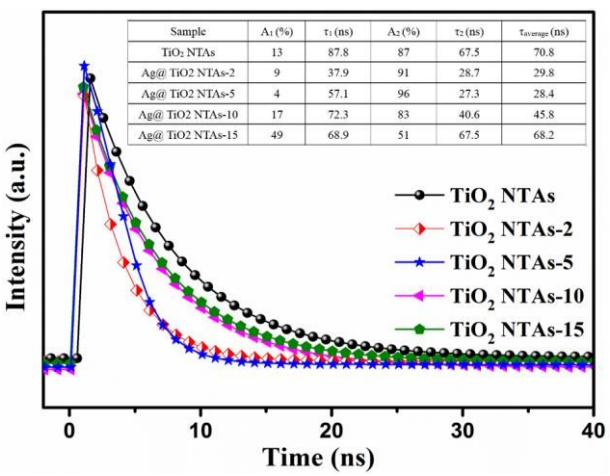

Figure 6. Time-resolved photoluminescence decay transients for the TiO_2 NTAs and Ag@TiO_2 NTAs with different deposition time.

The separation of photogenerated electron-hole pairs was evaluated by measuring the photocurrent. Figure 7 showed the current-voltage (I-v) and the current-time (I-t) characteristics of pure TiO_2 NTAs and Ag@TiO_2 NTAs-2, 5, 10 and 15 electrodes recorded in 0.1 M Na_2SO_4 under visible light irradiation. In Figure 7a, the photocurrent of bare TiO_2 NTAs electrodes was negligible. After the Ag nanoparticles were directly deposited on TNTs, the photocurrent density of Ag@TiO_2 NTAs raised with the increasing of bias potential ranging from -0.4 V to 0.4 V, as a result of the improved distribution of the Ag nanoparticles for the effective separation of the photogenerated electron-hole pairs. Notably, the deposition of Ag nanoparticles also conduced to the negative shift of flat band potential, indicating a shift in Fermi level to more negative potential. This confirms that Ag nanoparticles depositing can prolong the lifetime of the photogenerated carriers.[60,61] As shown in Figure 7b, when the pure TiO_2 NTAs electrode was under visible-light irradiation, there was a photocurrent density with ca. 0.001 mA cm^{-2}. However, the photocurrent density of the Ag@TiO_2 NTAs with different deposition time for 2, 5, 10 and 15 min was 0.024 mA cm^{-2}, 0.035 mA cm^{-2}, 0.005 mA cm^{-2}, 0.002 mA cm^{-2} which was approximately 24 times, 35 times, 5 times, 2 times higher than that of TiO_2 NTAs electrode at 0.3 V, respectively. The enhanced photocurrent could be ascribed to the decoration of Ag into the TiO_2 NTAs system, resulting in higher separation efficiency of the photogenerated electron-hole pairs and enhanced visible light absorption due to SPR effect.

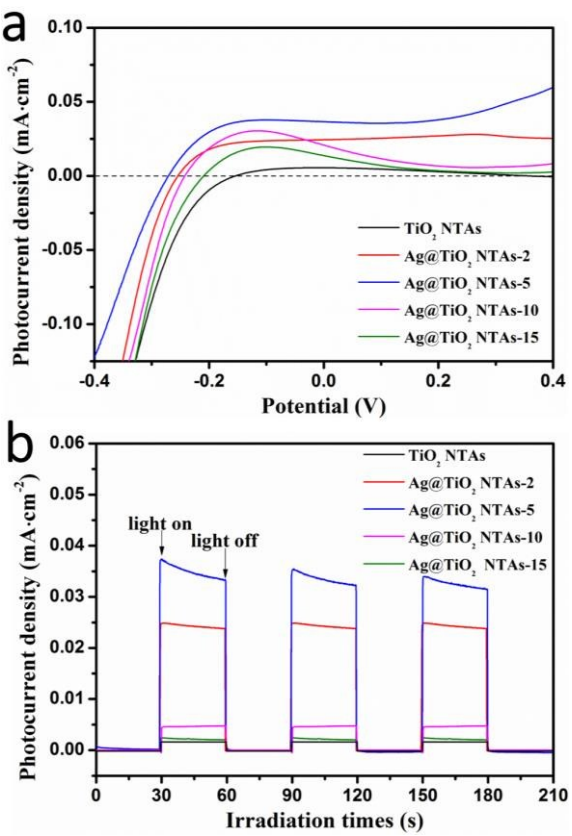

Figure 7. (a) Current-voltage characteristic and (b) photocurrent responses of as-prepared pure TiO_2 NTAs and Ag@TiO_2 NTAs with different deposition time for 2, 5, 10 and 15 min under visible light irradiation in 0.1 M Na_2SO_4 solution recorded at 0.3 V. The illumination from a 150 W Xe lamp (with a UV-light cutoff filter) was interrupted every 30 s.

The electrochemical impedance spectroscopy (EIS) measurements were verified to be an effective tool for scrutinizing the interfacial properties between the electrode (i.e., TiO_2 NTAs annealed at 450 ℃ and Ag@TiO_2 NTAs-5) and the electrolyte over a frequency range from 1×10^5 Hz to 0.1 Hz with a low open circuit potential both in the dark and under visible light illumination. The diameter of semicircle in the Nyquist plots at high frequency reflects the charge transfer process, and the smaller diameter of semicircle represents the lower charge transfer resistance.[62] As shown in Figure 8, the diameters of TiO_2 NTAs at 450 ℃ were much larger than those of Ag@TiO_2 NTAs-5 in the dark as well as under visible light irradiation. This supported that the Ag decoration considerably facilitated the electron mobility by reducing the recombination of electron-hole pairs and enhanced photocatalytic hydrogen production activity.

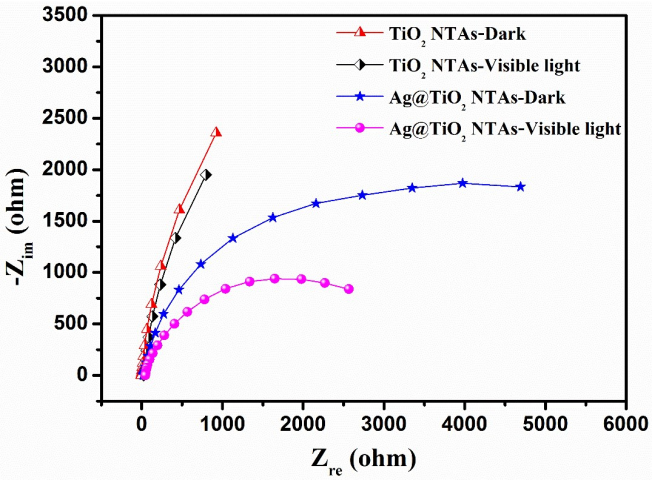

Figure 8. Electrochemical impedance spectra of TiO_2 NTAs at 450 ℃ and Ag@TiO_2 NTAs with deposition time for 5 min in the dark and under visible light illumination, respectively.

To evaluate the photoelectrocatalytic activity of the Ag@TiO_2 NTAs, photoelectrocatalytic hydrogen production experiment was conducted under 500 W Xe lamp with a UV light cutoff filter ($\lambda \geq$ 420 nm) with light intensity of 80 mW cm^{-2}. Figure 9a shows the hydrogen production rates of TiO_2 NTAs and Ag@TiO_2 NTAs with different deposition time for photoelectrocatalytic water splitting. When using the pure TiO_2 NTAs as the photocatalyst, the hydrogen production rate was only 2 μmol cm^{-2} h^{-1}. However, it was found that the hydrogen production rate of Ag@TiO_2 NTAs with different deposition time for 2, 5, 10, 15 min was about 20, 30, 14, 10 μmol cm^{-2} h^{-1}, respectively. Especially, the hydrogen production rate of the optimized Ag@TiO_2 NTAs with deposition time 5 min (30 μmol cm^{-2} h^{-1}) was 15 times higher than the pure TiO_2 NTAs counterpart (2 μmol cm^{-2} h^{-1}), indicating that the Ag nanoparticles sensitized on the TiO_2 NTAs with enhanced visible light absorption and the efficient separation of photogenerated charges improved the photocatalytic hydrogen production activity due to SPR effect. Beside the excellent photocatalytic water splitting performance, the Ag@TiO_2 NTAs also exhibited good stability of photocatalytic hydrogen production activity. As shown in Figure 9b, the amount of hydrogen production of Ag@TiO_2 NTAs with deposition time for 5 min had a little reduction within 5% after 5 cycles. This indicated that the Ag@TiO_2 NTAs remained active for long-term service without obvious deactivation.

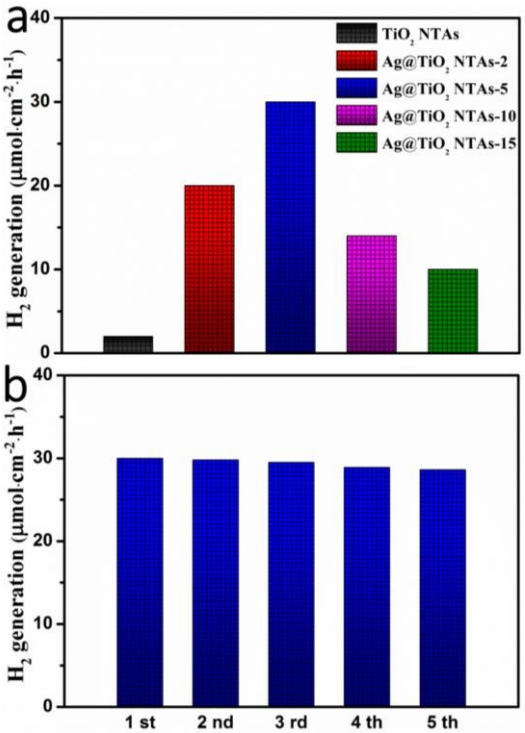

Figure 9. (a) Photoelectrocatalytic hydrogen production rate of the as-prepared samples in distilled water containing 20 vol% methanol under 500 W Xe lamp (80 mW cm^{-2}) with a UV light cutoff filter (b) Cycling hydrogen production curve of the prepared Ag@TiO_2 NTAs with deposition time for 5 min.

The markedly enhanced photocatalytic activity for hydrogen production was a direct consequence of synergetic effects of the highly ordered nanotubular TiO_2 structure and uniformly dispersed Ag nanoparticles. In order to describe how Ag@TiO_2 NTAs enhanced the photocatalytic hydrogen production activity, the energy band structure and electron-hole pairs separation was illustrated in Scheme 2. Upon visible light illumination, Ag nanoparticles could be photo-excited and generate a lot of electrons on its surface due to the surface plasmon resonance. Besides, a Schottky barrier was formed at Ag@TiO_2 NTAs interfaces due to the large work function, so charge separation was accompanied by photo-excited electrons easily transfer from the Ag nanoparticles to the conduction band of TiO_2 NTAs. Simultaneously, the SPR effect can form a strong local electronic field to enhance the energy of trapped electrons, making

them transfer and react with electron acceptors more easily.[63-65] Therefore, the conduction of TiO_2 NTAs can function as active sites for H_2 production, while the sacrificial reagent methanol as electron donors presented an oxidation on holes generating hydrogen ions, improving the stability of the Ag@TiO_2 NTAs samples and enhancing the photocatalytic hydrogen production activity.[66]

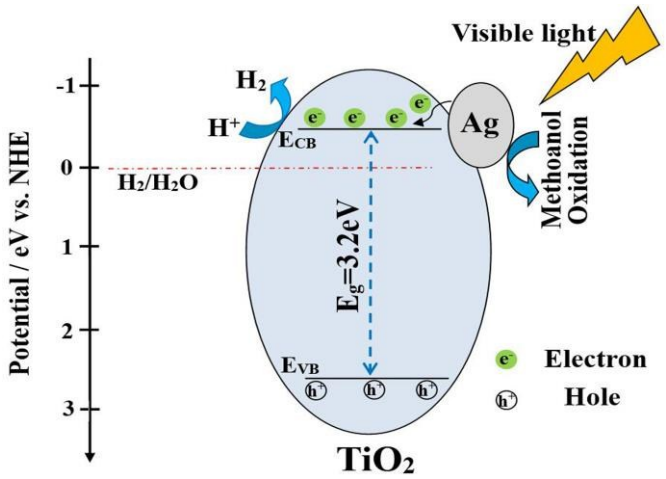

Scheme 2. Schematic diagram showing the energy band structure and electron-hole pairs separation in Ag@TiO_2 NTAs under visible light irradiation.

Conclusions

In summary, we have developed a very promising strategy of ultrasonication-assisted in situ deposition technique to realize highly uniform Ag nanoparticles dispersed on both inside and outside of the vertically aligned TiO_2 nanotubes. Such novel Ag@TiO_2 NTAs substantially enhanced the light absorption, increased the photogenerated electron-hole separation/transfer and notably improved photocatalytic hydrogen production activity under visible light illumination (15 times over the pristine TiO_2 NTAs counterpart). Therefore, this study provides an effective synthetic strategy to uniformly synthesize nanoparticle-modified one-dimensional heterostructures which have promising applications in environmental reclamation and energy harvest.

Acknowledgements

The authors thank the National Natural Science Foundation of China (21501127, 51502185 and 51373110), Natural Science Foundation of Jiangsu Province of China (BK20130313; BK20140400), Deanship of Scientific Research at King Saud University (PRG-1436-03). We also acknowledge the funds from the project of the Priority Academic Program Development of Jiangsu Higher Education Institutions (PAPD), and Project for Jiangsu Scientific and Technological Innovation Team (2013).

Notes and references

[a]National Engineering Laboratory for Modern Silk, College of Textile and Clothing Engineering, Soochow University, Suzhou 215123, China.
[b]School of Materials Science and Engineering, Nanyang Technological University, 50 Nanyang Avenue, 639798, Singapore.
[c]School of Materials Science and Engineering, University of Science and Technology Beijing, Beijing 100083, China.
[d]Research Center of Cooperative Innovation for Functional Organic / Polymer Material Micro/Nanofabrication, Soochow University, Suzhou, Jiangsu 215123, China.
[e]Petrochemical Research Chair, Department of Chemistry, College of Science, King Saud University, Riyadh 11451, Saudi Arabia.

Corresponding author email: jyhuang81@suda.edu.cn; kqzhang@suda.edu.cn; yklai@suda.edu.cn.

Electronic Supplementary Information (ESI) available: [EDS and mapping spectra of Ag@TiO_2 NTAs ultrasonication-assisted deposition time for 5 min, the size distribution of Ag nanoparticles Ag@TiO_2 NTAs with different deposition time, SEM images and EDS spectra of TiO_2 NTAs with ultrasonication-assisted deposition time for 5 min with 5, 20, and 40 mM $AgNO_3$, photocurrent responses and hydrogen production rate of as-prepared pure TiO_2 NTAs and Ag@TiO_2 NTAs with ultrasonication-assisted deposition time for 5 min with different concentration of $AgNO_3$. See DOI: 10.1039/b000000x/

1. L. L. Zhu, M. H. Hong and G. W. Ho, *Nano Energy*, 2015, **11**, 28-37.
2. M. D. Ye, M. Y. Wang, D. J. Zheng, N. Zhang, C. J. Lin and Z. Q. Lin, *Nanoscale*, 2014, **6**, 3576-3584.
3. A. Fujishima and K. Honda, *Nature*, 1972, **238**, 37-38.
4. M. Z. Ge, C. Y. Cao, J. Y. Huang, S. H. Li, S. N. Zhang, S. Deng, Q. S. Li, K. Q. Zhang and Y. K. Lai, *Nanotechnol. Rev.*, 2016, **5**, DOI: 10.1515/ntrev-2015-0049.
5. Z. H. Zhao, J. Tian, Y. H. Sang, A. Cabot and H. Liu, *Adv. Mater.*, 2015, **27**, 2557-2582.
6. M. Y. Wang, J. Ioccozia, L. Sun, C. J. Lin and Z. Q. Lin, *Energy Environ. Sci.*, 2014, **7**, 2182-2202.
7. D. Ying, M. Y. Wang, B. Zhou, G. L. Zhang and Z. Q. Lin, *Nanoscale*, 2015, **7**, 12990-12997.
8. M. Z. Ge, C. Y. Cao, J. Y. Huang, S. H. Li, Z. Chen, K. Q. Zhang, S. S. Al-Deyab and Y. K. Lai, *J. Mater. Chem. A*, 2016, **4**, DOI: 10.1039/C5TA09323F.
9. S. Hao, J. Deng, L. B. Qiu, X. Fang and H. S. Peng, *Energy Environ. Sci.*, 2015, **8**, 1139-1159.
10. W. X. Guo, C. Xu, G. Zhu, C. F. Pan, C. J. Lin and Z. L. Wang, *Nano Energy*, 2012, **1**, 176-182.
11. M. D. Ye, H. Y. Liu, C. J. Lin and Z. Q. Lin, *Small*, 2013, **9**, 312-321.
12. Y. X. Tang, Y. Y. Zhang, J. Y. Deng, D. P. Qi, W. R. Leow, J. Q. Wei, S. Y. Yin, Z. L. Dong, R. Yazami, Z. Chen and X. D. Chen, *Angew. Chem. Int. Ed.*, 2014, **126**, 13706-13710.
13. Y. X. Tang, Y. Y. Zhang, J. Y. Deng, J. Q. Wei, H. L. Tam, B. K. Chandran, Z. L. Dong, Z. Chen and X. D. Chen, *Adv. Mater.*, 2014, **26**, 6111-6118.
14. Y. X. Tang, Y. Y. Zhang, W. L. Li, B. Ma and X. D. Chen, *Chem. Soc. Rev.*, 2015, **44**, 5926-5940.
15. Q. L. Wu, J. G. Xu, X. F. Yang, F. Q. Lu, S. M. He, J. L. Yang, H. J. Fan and M. M. Wu, *Adv. Energy Mater.*, 2015, **5**, 1401756.
16. G. M. Wang, H. Y. Wang, Y. C. Ling, Y. C. Tang, X. Y.

Yang, R. C. Fitzmorris, C. C. Wang, J. Z. Zhang and Y. Li, *Nano Lett.*, 2011, **11**, 3026-3033.
17. C. T. Li, S. R. Li, L. Y. Chang, C. P. Lee, P. Y. Chen, S. S. Sun, J. J. Lin, R. Vittal and K. C. Ho, *J. Mater. Chem. A*, 2015, **3**, 4695-4705.
18. Q. Kang, J. Y. Cao, Y. J. Zhang, L. Q. Liu, H. Xu and J. H. Ye, *J. Mater. Chem. A*, 2013, **1**, 1 5766-5774.
19. Z. Wu, Y. F. Su, J. D. Yu, W. Xiao, L. Sun and C. J. Lin, *Int. J. Hydrogen Energ.*, 2015, **40**, 9704-9712.
20. M. M. Momeni and Y. Ghayeb, *J. Alloys Compd.*, 2015, **637**, 393-400.
21. M. M. Momeni, Y. Ghayeb and Z. Ghonchegi, *Ceram. Int.*, 2015, **41**, 8735-8741.
22. G. K. Mor, K. Shankar, M. Paulose, O. K. Varghese and C. A. Grimes, *Nano Lett.*, 2005, **5**, 191-195.
23. H. Z. Gao, H. G. Wang, Y. L. Jin, J. Lv, G. Q. Xu, D. M. Wang, X. Y. Zhang, Z. Chen, Z. X. Zheng and Y. C. Wu, *Phys. Chem. Chem. Phys.*, 2015, **17**, 17755-17761.
24. J. Tian, Z. H. Zhao, A. Kumar, R. I. Boughton and H. Liu, *Chem. Soc. Rev.*, 2014, **43**, 6920-6937.
25. M. D. Ye, J. J. Gong, Y. K. Lai, C. J. Lin and Z. Q. Lin, *J. Am. Chem. Soc.*, 2012, **134**, 15720-15723.
26. M. M. Momeni and Y. Ghayeb, *J. Electroanal. Chem.*, 2015, **751**, 43-48.
27. N. T. Nguyen, M. Altomare, J. Yoo and P. Schmuki, *Adv. Mater.*, 2015, **27**, 3208-3215.
28. K. F. Huo, B. Gao, J. J. Fu, L. Z. Zhao and P. K. Chu, *RSC Adv.*, 2014, **4**, 17300-17324.
29. M. M. Momeni, Y. Ghayeb and Z. Ghonchegi, *J. Solid State Electrochem.*, 2015, **19**, 1359-1366.
30. H. L. Tang, M. Xiong, D. Y. Qu, D. Liu, Z. J. Zhang, Z. Z. Xie, X. Wei, W. M. Tu and D. Y. Qu, *Nano Energy*, 2015, **15**, 75-82.
31. G. S. Li, L. Wu, F. Li, P.P. Xu, D. Q. Zhang and H. X. Li, *Nanoscale*, 2013, **5**, 2118-2125.
32. M. Y. Wang, L. Sun, Z. Q. Lin, J. H. Cai, K. P. Xie and C. J. Lin, *Energy Environ. Sci.*, 2013, **6**, 1211-1220.
33. M. M. Momeni, Y. Ghayeb and M. Davarzadeh, *J. Electroanal. Chem.*, 2015, **739**, 149-155.
34. J. Li, W. J. Wang, L. Zhao, L. Rong, S. J. Lan, H. C. Sun, H. Zhang and B. Yang, *ACS Appl. Mater. Interfaces*, 2015, **7**, 11613-11623.
35. Y. T. Yen, C. W. Chen, M. Fang, Y. Z. Chen, C. C. Lai, C. H. Hsu, Y. C. Wang, H. Lin, C. H. Shen, J. M. Shieh, J. C. Ho and Y. L. Chueh, *Nano energy*, 2015, **15**, 470-478.
36. X. T. Wang, C. H. Liow, A. Bisht, X. F. Liu, T. C. Sum, X. D. Chen and S. Z. Li, *Adv. Mater.*, 2015, **27**, 2207-2214.
37. Z. F. Jiang, D. Liu, D. L. Jiang, W. Wei, K. Qian, M. Chen and J. M. Xie, *Dalton Trans.*, 2014, **43**, 13792-13802.
38. Z.F. Jiang, X.M. Lv, D.L. Jiang, J.M. Xie, D.J. Mao, *J. Mater. Chem. A*, 2013, **1**, 14963-14972.
39. W. T. Jiang, N. Ullah, G. Divitini, C. Ducati, R. V. Kumar, Y. C. Ding and Z. H. Barber, *Langmuir*, 2012, **28**, 5427-5431.
40. W. T. Chang, Y. C. Hsueh, S. H. Huang, K. I. Liu, C. C. Kei and T. P. Perng, *J. Mater. Chem. A*, 2013, **1**, 1987-1991.
41. K. P. Xie, L. Sun, C. L. Wang, Y. K. Lai, M. Y. Wang, H. B. Chen and C. J. Lin, *Electrochim. Acta*, 2010, **55**, 7211-7218.
42. Y. K. Lai, H. F. Zhuang, K. P. Xie, D. G. Gong, Y. X. Tang, L. Sun, C. J. Lin and Z. Chen, *New. J. Chem.*, 2010, **34**, 1335-1340.
43. Y. X. Tang, Z. L. Jiang, J. Y. Deng, D. G. Gong, Y. K. Lai, H. T. Tay, I. T. K. Joo , T. H. Lau , Z. L. Dong and Z. Chen, *ACS Appl. Mater. Inter.*, 2012, **4**, 438-446.
44. N. Mohaghegh, M. Faraji, F. Gobal and M. R. Gholami, *RSC Adv.*, 2015, **5**, 44840-44846.
45. Q. Y. Li, R. Li, L. L. Zong, J. H. He, X. D. Wang and J. J. Yang, *Int. J. Hydorgen. Energ.*, 2013, **38**, 12977-12983.
46. C. B. Liu, C. H. Cao, X. B. Luo and S. L. Luo, *J. Hazard. Mater.*, 2015, **285**, 319-324.
47. L. Sun, J. Li, C. L. Wang, S. F. Li, Y. K. Lai, H. B. Chen and C. J. Lin, *J. Hazard. Mater.*, 2009, **171**, 1045-1050.
48. D. Wang, Z. H. Zhou, H. Yang, K. B. Shen, Y. Huang and S. Shen, *J. Mater. Chem.*, 2012, **22**, 16306-16311.
49. M. Y. Wang, L. Sun, J. H. Cai, P. Huang, Y. F. Sun and C. J. Lin, *J. Mater. Chem. A*, 2013, **1**, 12082-12087.
50. M. Z. Ge, S. H. Li, J. Y. Huang, K. Q. Zhang, S. S. Al-Deyab and Y. K. Lai, *J. Mater. Chem. A*, 2015, **3**, 3491-3499.
51. Z. Wu, Y. Y. Wang, L. Sun, Y. X. Mao, M.Y. Wang and C. J. Lin, *J. Mater. Chem. A*, 2014, **2**, 8223-8229.
52. W. Y. Gao, M. Q. Wang, C. X. Ran, X. Yao, H. H. Yang, J. Liu, D. L. He and J. B. Bai, *Nanoscale*, 2014, **6**, 5498-5508.
53. J. He, I. Ichinose, T. Kunitake and A. Nakao, *Langmuir*, 2002, **18**, 10005-10010.
54. M. Z. Ge, C. Y. Cao, S. H. Li, S. N. Zhang, S. Deng, J. Y. Huang, Q. S. Li, K. Q. Zhang, S. S. Al-Deyab and Y. K. Lai, *Nanoscale*, 2015, **7**, 11552-11560.
55. Y. Zhang, X. Li, X. Hua, N. Ma, D. Chen and H. Wang, *Scr. Mater.*, 2009, **61**, 296-299.
56. P. H. Wang, Y. X. Tang, Z. L. Dong, Z. Chen and T. T. Lim, *J. Mater. Chem. A*, 2013, **1**, 4718-4727.
57. R. K. Kokal, P. N. Kumar, M. Deepa and A. K. Srivastava, *J. Mater. Chem. A*, 2015, **3**, 20715-20726.
58. Y. Y. Zhang, Y. X. Tang, X. F. Liu, Z. L. Zhi, H. H. Hng, Z. Chen, T. C. Sum and X. D. Chen, *Small*, 2013, **9**, 996-1002.
59. X. T. Wang, C. H. Liow, A. Bisht, X. F. Liu, T. C. Sum, X. D. Chen and S. Z. Li, *Adv. Mater.*, 2015, **27**, 2207-2214.
60. J. Luo, L. Ma, T. He, C. F. Ng, S. Wang, H. Sun and H. J. Fan, *J. Phys. Chem. C*, 2012, **116**, 11956-11963.
61. L. Sun, J. Cai, Q. Wu, P. Huang, Y. Su and C. J. Lin, *Electrochim. Acta*, 2013, **108**, 525-531.
62. M. Y. Wang, D. J. Zheng, M. D. Ye, C. C. Zhang, B. B. Xu, C. J. Lin, L. Sun and Z. Q. Lin, *Small*, 2015, **11**, 1436-1442.
63. Y. Wang, J. G. Yu, W. Xiao and Q. Li, *J. Mater. Chem. A*, 2014, **2**, 3847-3855.
64. Z. Y. Zhan, J. N. An, H. C. Zhang, R. V. Hansen and L. X. Zheng, *ACS Appl. Mater. Interfaces*, 2014, **6**, 1139-1144.
65. Y. H. Chen, J. J. Bian, L. L. Qi, E. Z. Liu and J. Fan, *J. Nanomater.*, 2015, **2015**, 905259.
66. S. Oros-Ruiz, R. Zanellaa, R. López, A. Hernández-Gordillo and R. Gómez, *J. Hazard. Mater.*, 2013, **263**, 2-10.

Graphical Abstract:

An ultrasonication-assisted in situ deposition strategy was developed to realize uniform Ag nanoparticles dispersed on TiO_2 nanotube arrays ($Ag@TiO_2$ NTAs). Attributed to the synergist effect between the surface plasmon resonance of Ag for enhanced visible-light absorption and facilitated photogenerated electron-hole separation/transfer, $Ag@TiO_2$ NTAs exhibited greatly enhanced photocatalytic hydrogen production activity than that of the pristine TiO_2 NTAs.